Preprints.org

Article

Not peer-reviewed version

Synthesis and Assessment of a Polyurethane Carrier Used for the Transmembrane Transfer of 2'-Deoxycytidine-5'-monophosphate sodium salt

Florin Borcan * , Titus Vlase , Gabriela Vlase , Roxana Popescu , Codruta M Soica

Posted Date: 1 August 2023

doi: 10.20944/preprints202308.0025.v1

Keywords: cells culture; drug delivery; FT-IR; mice skin; thermal analysis; UV-Vis; Zetasizer

Preprints.org is a free multidiscipline platform providing preprint service that is dedicated to making early versions of research outputs permanently available and citable. Preprints posted at Preprints.org appear in Web of Science, Crossref, Google Scholar, Scilit, Europe PMC.

Copyright: This is an open access article distributed under the Creative Commons Attribution License which permits unrestricted use, distribution, and reproduction in any medium, provided the original work is properly cited.

Preprints (www.preprints.org) | NOT PEER-REVIEWED | Posted: 1 August 2023 doi:10.20944/preprints202308.0025.v1

Disclaimer/Publisher's Note: The statements, opinions, and data contained in all publications are solely those of the individual author(s) and contributor(s) and not of MDPI and/or the editor(s). MDPI and/or the editor(s) disclaim responsibility for any injury to people or property resulting from any ideas, methods, instructions, or products referred to in the content.

Article

Synthesis and Assessment of a Polyurethane Carrier Used for the Transmembrane Transfer of 2'-Deoxycytidine-5'-Monophosphate Sodium Salt

Florin Borcan [1,*], Titus Vlase [2], Gabriela Vlase [2], Roxana Popescu [3] and Codruta M Soica [4]

[1] Department I, Advanced Instrumental Screening Center, Faculty of Pharmacy, "Victor Babes" University of Medicine and Pharmacy, 2 E. Murgu Sq., Timisoara-300041, Romania
[2] Research Center "Thermal analysis in environmental problems", Faculty of Chemistry, Biology, Geography, West University of Timisoara, 16 Pestalozzi Str., Timisoara-300115; titus.vlase@e-uvt.ro (T.V.); gabriela.vlase@e-uvt.ro (G.V.)
[3] Department II, Faculty of Medicine, "Victor Babes" University of Medicine and Pharmacy, 14A T. Vladimirescu Str., Timisoara-300041, Romania; popescu.roxana@umft.ro
[4] Department II, Faculty of Pharmacy, "Victor Babes" University of Medicine and Pharmacy, 2 E. Murgu Sq., Timisoara-300041, Romania; codrutasoica@umft.ro
* Correspondence: fborcan@umft.ro; Tel.: 0040-722-371-025

Abstract: The drug delivery systems receive more and more attention for the control and treatment of many diseases due to their increased number in recent years. The main aims of this study were to develop and to characterize a polyurethane drug delivery system that it is intended to be used for the transmembrane transport of nucleosides. Three different samples have been synthesized based on aliphatic diisocyanates (hexamethylene diisocyanate, isophorone diisocyanate and lysine diisocyanate) as organic phase, respectively a mixture of polyethylene glycol, polycaprolactone diol and low molecular weight diols as aqueous phase. The samples were characterized by pH, refractivity index and solubility measurements, drug loading efficacy and release investigations, thermal behavior, Zetasizer, cells viability and irritation tests on mice skin. The results indicate the obtaining of different populations of neutral acido-basic particles with size between 132 and 190 nm; the Zeta potential values and SEM images show a medium tendency to form clusters, while UV-Vis evaluations indicate an almost 70% encapsulation efficacy, a prolonged release (45% of encapsulated substance is released in the first 5 days) and around 70% of particles have penetrated an artificial membrane in the first 24h. The synthesized products can be tested in further clinical trials, the currently tests on cells culture and mice skin revealing no side effects.

Keywords: cells culture; drug delivery; FT-IR; mice skin; thermal analysis; UV-Vis; Zetasizer

1. Introduction

Nucleosides represent a large group of biological molecules known as glycosylamines displaying similar structures with nucleotides but lacking phosphate functional groups. They exhibit very diverse structures containing a nucleobase or nitrogenous base (adenine, thymine, cytosine, guanine) that is covalently linked to a monosaccharide with five carbon atoms [1,2]. The nucleosides act as precursors in the synthesis of nucleic acids, and they are also involved in the control of the metabolism and growth of all living cells; additionally, they modulate certain activities of the muscular, cardiovascular, and nervous systems [3]. Various supplements based on exogenous nucleosides (and nucleotides) have been developed for the patients who lack the ability to synthesize these compounds *de novo* [4]. The challenges and advantages associated with the use of drug delivery systems for nucleosides can also be associated to various approaches for cancer treatment [5,6]. 2′-Deoxycytidine-5′-monophosphate (dCMP, Figure 1), often found as a substrate of uridine monophosphate, is a compound that contains cytosine (2-oxy-4-amino-pyrimidine) as the

© 2023 by the author(s). Distributed under a Creative Commons CC BY license.

Preprints (www.preprints.org) | NOT PEER-REVIEWED | Posted: 1 August 2023 doi:10.20944/preprints202308.0025.v1

nitrogenous base linked to a deoxyribose and a phosphate group; in the DNA double helix dCMP is paired with deoxyguanosine-monophosphate (dGMP) [7]. The reactivity in water, the functionalization and the encapsulation of its salts were highly investigated in the last two decades to enhance its bioavailability [8,9].

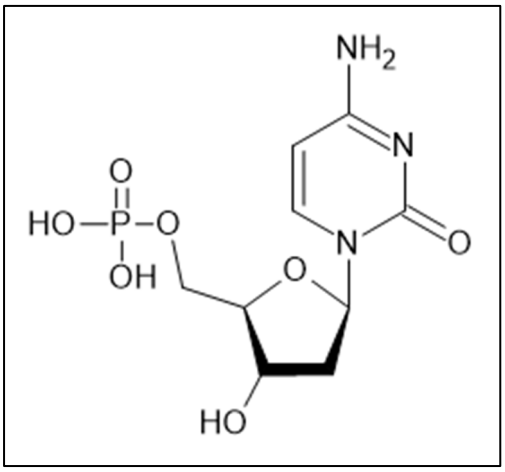

Figure 1. The chemical structure of dCMP.

Polyurethane (PU) drug delivery systems consist of a small group of nano- and micro-particles, capsules, and structures that were developed starting with the last decade of the last century. Although this polymer class was initially developed industrially (as foams, adhesives and coatings), in the second part of the last century various biomedical applications began to appear due to the versatility, lack of toxicity and hemocompatibility of the finished products [10–12]. The first syntheses of polyurethane carriers were based on aromatic compounds (methylene-diphenyl diisocyanate or MDI and toluene diisocyanate or TDI) and resulted in large structures with low penetration rates; hence, it was necessary to find a synthesis method able to reduce the carrier size. Several studies by K. Bouchemal et al. [13–15] describe colloidal suspensions of polyurethane capsules with much smaller sizes than their predecessors; their synthesis, based on an interfacial polyaddition process combined with a spontaneous emulsification, used a mixture of polyethylene glycol, ethylene glycol, butanediol, and hexanediol as aqueous phase, isophorone diisocyanate, and two surfactants (a hydrophilic one, Tween® 20, and a lipophilic one, Span® 85).

Our research team has synthesized and characterized different polyurethane structures that can be used as carriers for various extracts [16–18] and drugs [19–21] in the last 15 years; the recipe of the synthesis and the raw materials have been continuously modified, ensuring that the size of the particles allows for the most efficient encapsulation and an easy-to-control release time. On the other hand, we managed to reduce the number of precursors, by eliminating one of the surfactants and the catalyst, thus reducing the toxicity potential while maintaining optimal surface charge values in order to prevent particle agglomeration. To the best of our knowledge, the presence of polyurethanes as carriers for nucleosides and nucleic acids is very limited; therefore, the main aim of the current study was to obtain and characterize an efficient and safe polyurethane drug delivery system suitable for the transmembrane transfer of nucleosides.

2. Materials and Methods

2.1. Materials and animals

Tween® 20 and hexamethylene diisocyanate (HDI) were purchased from Merck (Darmstadt, Germany), isophorone diisocyanate (IPDI), polyethylene glycol (PEG 400), polycaprolactone diol (PCL Mn~530), 1,6-hexanediol (HD), tris(hydroxymethyl)amino-methane (THAM), inorganic salts (NaCl, KCl and $MgCl_2$, Na_2HPO_4, K_2HPO_4, KH_2PO_4 and $NaHCO_3$) and 2′-Deoxycytidine 5′-monophosphate as sodium salt were acquired from Sigma Aldrich (St Louis, USA). Lysine

Preprints (www.preprints.org) | NOT PEER-REVIEWED | Posted: 1 August 2023 doi:10.20944/preprints202308.0025.v1

diisocyanate (LDI) was obtained from Imaginechem Co. (Hangzhou, China Rep.) and acetone from Honeywell Riedel-de Haen (Seelze, Germany). All the reagents were analytical grade purity and they were used without any previous purification; double distilled water was prepared in-house using a JP Selecta Dest-4 distiller.

For the *in vitro* experiments using cells culture, HDFa (Human Dermal Fibroblast) was purchased from Invitrogen (Waltham, USA), while the reagents (culture media, fetal bovine serum (FBS), antibiotics, phosphate buffered saline (PBS), 0.25% trypsin-EDTA solution, MTT solution, dimethylsulfoxide) and culture supplies (culture flasks, Pasteur pipettes, pipette tips, conical tubes, 96-well microplates) were achieved from Thermo Fischer Scientific (Waltham, USA).

Male, 7-9-week-old CB17SCID and Nu/Nu, Balb-c mice were purchased from Charles River (Sulzfeld, Germany). Mice were kept under standard conditions - temperature (23±2 ˚C), humidity (50-60%), 12h light/dark cycle; they were fed *ad libitum*. The animals were not euthanized at the end of this experiment due to their health condition and they were used later in other experiments.

2.2. Synthesis of the PU carriers

The synthesis of the drug delivery system is based on an exothermic polyaddition reaction between an active hydrogen-containing phase (mixture of different ether and/or ester polyols) and a diisocyanate. In this study, aliphatic isocyanates (hexamethylene diisocyanate, isophorone diisocyanate and lysine diisocyanate) have been chosen in order to avoid the carcinogenic risk of aromatic compounds. The mixture of polyols (PEG 400 and PCL) and their ratio were established according to our previous results [22,23] taking into consideration that the balance between the ether and ester polyols has a major impact on the drug release kinetics.

The active hydrogen-containing phase (a mixture of 1.75 mL HD, 3.50 g PEG 400, 3.10 g PCL, 1.15 g THAM and 0.50 g 2′-Deoxycytidine 5′-monophosphate sodium salt) and 90 mL of double distilled water were added to a Duran® beaker and stirred on a Velp hot plate stirrer (Usmate, Italy) at 350 rpm and 35±0.2 ˚C overnight. In parallel, three isocyanates solutions obtained from 6.00 mL HDI, IPDI, and LDI, respectively, in 50.00 mL acetone, were homogenized in three cone-shaped flasks at 350 rpm and 40±0.2 ˚C for 30 minutes. Then, the content of the beaker was divided equally among the three flasks and their contents continued to be stirred at 350 rpm and 40±0.2 ˚C for 3 hours to complete the synthesis of the macromolecular chains; the temperatures were precisely monitored using a P700 Universal thermometer from Dostmann electronic GmbH (Wertheim, Germany). In the end, the content of the three flasks was sonicated for 5 min using a Bandelin Sonorex Digitec bath sonicator (Berlin, Germany). The three samples were labeled as follows: str 1 (based on HDI), str 2 (based on IPDI) and str 3 (based on LDI).

The obtained suspensions were repeatedly washed with a mixture of water-acetone (1: 1.4, v/v), were passed through 0.22 μm PVDF sterile syringe filters from Merck Millipore (Darmstadt, Germany) and then centrifuged at 2000 G using an Ika Mini G microcentrifuge (Staufen, Germany) in order to concentrate the samples; the mixture used to wash the samples was later analyzed in order to established the free drug content. Finally, the samples were dried in borosilicate glass Petri dishes at 45 ˚C inside a PolEko SL115 drying oven to constant mass (almost 30 hours).

2.3. Samples Stability

The stability of PU carriers was evaluated as previously described [16]: briefly, an aliquot of every sample was maintained at 3 different temperatures, respectively (8±0.5 ˚C in a refrigerator, 25±0.5 and 40±0.5 ˚C with 65±3% relative humidity in a laboratory incubator) for 30 days; various parameters as color, electrical conductivity and pH were recorded every third day. The color stability was evaluated using the changes of Amax and a SI Analytics UVi Line 9400 spectrophotometer (Mainz, Germany), while the electrical conductivity was assessed using a Jenway Bench 4010 Conductivity meter (Staffordshire, UK) at 25 ˚C in aqueous solutions (0.8 mg mL^{-1}).

Preprints (www.preprints.org) | NOT PEER-REVIEWED | Posted: 1 August 2023 doi:10.20944/preprints202308.0025.v1

2.4. pH, Refractive index and Solubility Measurements

The sample pH was evaluated using a Mettler Toledo FiveGo F2 portable pH meter (Schwerzenbach, Switzerland), InLab® Expert Go Sensor and aqueous solutions with the same concentration (0.8 mg mL^{-1}) at the same temperature (25 °C). The instrument was previously calibrated using four different buffer solutions (pH= 4.01, 7, 9.21 and 11) provided by the same manufacturer.

The refractive index of the synthesized samples was obtained using 2-3 drops of every aqueous solutions on a Kern digital refractometer (Balingen, Germany) at room temperature.

A series of dissolution tests were conducted in distilled water, acetone, and DMSO, respectively, following a procedure already described in the literature [17]: 5.0 mg dried powder were dissolved in the respective solvent in 20 mL glass vials with screw caps at room temperature; the volume of every solvent was registered when a single, clear liquid phase with no distinct solid or gel particles was recorded.

2.5. Drug Loading

The amount of 2'-Deoxycytidine-5'-monophosphate sodium salt successfully entrapped inside the carrier particles was found by reporting the quantity of the free drug to the total added amount. The amounts were calculated using the Beer–Lambert law at 271 nm and a SI Analytics UVi Line 9400 Spectrophotometer (Mainz, Germany); a calibration curve by plotting the absorption values as a function of drug concentration was initially drawn and it can be described by Equation (1):

$$y = 0.1261\ x,\ R^2 = 0.9829 \quad (1)$$

where: y = absorption value, x = drug concentration (μg/mL) and R^2 = the coefficient of determination.

2.6. Drug Release Profile

The cumulative drug release (CDR) was calculated by measuring the amount of the active agent that was released during the carrier's exposure to simulated body fluid (SBF) prepared according to F. Baino and S. Yamaguchi [24]. First, the solution of SBF was prepared as follows: 6.55 g NaCl, 2.27 g $NaHCO_3$, 0.37 g KCl, 0.14 g Na_2HPO_4 were mixed with 960 mL double distilled water in a 1000 mL-capacity flat bottom flask and heated at 37 °C; then 0.31 g $MgCl_2$ hexahydrate, 0.37 g $CaCl_2$ dihydrate, 0.07 g Na_2SO4, 6.06 g Tris were added and the pH was adjusted to 7.4 with a solution HCl 1M. The samples were introduced into the degrading environment and kept for 5 days at 37 °C and 150 rpm; at specific time points (daily) 1.0 mL of SBF was replaced with fresh degrading environment and UV-Vis spectroscopy was employed to quantify the released drug.

2.7. The Penetrability Rate

A small *in vitro* Franz-type vertical static diffusion cell system (Φ 15 mm, diffusion area of 1.77 cm^2 and the receptor volume of 12.0 mL) and a PVDF artificial membrane Spectra/Por® were used to test the carrier permeation. The receptor compartment was filled with phosphate buffer saline in such a way that it would not remain air bubbles between the artificial membrane and the receptor fluid. The experiment was conducted at 25±1 °C, and at every 10 h, 1.0 mL liquid from the receptor compartment was replaced with fresh buffer and spectrophotometrically analyzed between 356 and 362 nm depending on the sample/diisocyanate type.

2.8. FTIR-UATR spectra

FTIR-UATR analysis was performed using a Shimadzu AIM-9000 device by employing the Attenuated Total Reflectance (ATR) technique without a preliminary sample preparation. The data was collected after 20 consecutive readings at a resolution of 4 cm^{-1}, within the 4000–280 cm^{-1} range.

Preprints (www.preprints.org) | NOT PEER-REVIEWED | Posted: 1 August 2023 doi:10.20944/preprints202308.0025.v1

2.9. Raman spectroscopy

The spectra were collected with a Raman spectrometer (Horiba Scientific, Kyoto, Japan): the samples were compressed with a hydraulic press to obtain circular discs and a 785 nm (red) laser with a deviation angle (DV) and a diffraction grating of 500 nm was used. The spectra were collected from Raman shift 30 to 2000 cm^{-1} using a 5× objective lens; each spectrum was obtained using an acq. time of 30 s and two accumulations.

2.10. Thermal Analysis

The thermal stability of samples was investigated using a Thermal Analyzer TGA/DSC3+ STARe System (Mettler Toledo, Port Melbourne, Australia). Analyses were performed between 25-500 °C in a dynamic air atmosphere (100 mL/min, synthetic air) with a 10°/min heating rate. Small amounts of every sample (between 3.5 and 4.5 mg) were placed in 40 µL aluminum melting crucibles with pin and sealed with pierced lids using a DSC-204 Netzsch differential scanning calorimeter (Selb, Germany) under the same conditions (atmosphere, heating rate and temperature range).

2.11. Zetasizer Tests

The size and surface charge of samples were evaluated through dynamic light scattering technique on a Cordouan Technol. system (Pessac, France) containing a nanosized detector (Vasco analyzer) and a charge detection module (Wallis). The following input parameters were set for the determination of particles size and its distribution: temperature (22 °C), time interval (18 µs), channels number (460), laser power (85%), acquisition mode (continuous) and analysis mode (Pade-Laplace). The following parameters were set to detect the surface charge: temperature (22 °C), applied field (automatic), resolution (0.8 Hz - medium), measures number/sequence (3), laser power (75%), Henry function (Smoluchowski), cuvettes (quartz with applicability between 190-2500 nm).

2.12. SEM Analysis

Sample morphology was assessed using a compact and versatile JSM-IT200 scanning electron microscope (Peabody, MA, USA). The following parameters were set: landing voltage (10.0 kV), WD (9.6 mm), magnification (1,400x), scan rotation (336.7 °) and pressure (40 Pa).

2.13. Cells Viability

HDFa cells (passage 3) were used for the experiment, the cells being seeded in a me-dium supplemented with 10% fetal bovine serum and 1% penicillin-streptomycin. Cells were grown under standard conditions in an incubator in the specific environment al-ready presented. The medium was changed regularly every 2-3 days. The proliferation of cells was determined by the MTT colorimetric technique. For the biocompatibility analysis of the compounds, cells from the HDFa line (5x10^5 cells/mL, respectively 5x10^4 cells/well) were seeded in 100 µL medium in 96-well plates. Cells were allowed to adhere for 24 hours in the incubator. After 24 hours, the growth medium was changed with the test compounds, diluted in the medium in different ratios: 90 µL medium+10 µL sample, 95 µL medium+5 µL sample, and 99 µL medium+1 µL sample. In parallel, we used con-trol batches of cells treated with the DMSO, in similar concentrations to those in the test samples. The tested samples were suspended in DMSO. All tests were performed in trip-licate. At 24, 48, and 72 hours after the treatment, the cell proliferation tests were per-formed using the MTT assay, and the absorbance at 590 nm was measuring using a Bio-Tek Synergy H1 spectrophotometer (Santa Clara, CA, USA).

The percentage of cell proliferation is described by Equation (2):

$$\text{Proliferation (\% control)} = (At / Ac) \times 100 \quad (2)$$

where *At* is the absorbance for the test solutions and *Ac* is the absorbance for the control. The average values for three consecutive determinations were used for the calculation.

Preprints (www.preprints.org) | NOT PEER-REVIEWED | Posted: 1 August 2023 doi:10.20944/preprints202308.0025.v1

2.14. Skin Irritation Evaluations

A pharmaco-toxicological evaluation for the newly synthesized products was performed using sensitive mice with and without hair. The mice were divided into five groups, labeled as the three PU carrier samples and two special groups (control group – mice treated only with the solvent, and SLS group – mice treated with a 2.0% sodium lauryl sulfate solution, a recognized skin irritant). The hair from the back of CB17SCID mice (3-4 square cm) was shaved at the beginning of experiment and then every 5 days. The application of the studied samples (40±3 µL once) was done on the back skin every third day for 15 days and the measurements of parameters were performed 30 minutes later by the same operator under the same conditions (temperature and humidity). The modification of skin erythema was monitored using a Mexameter® MX 18 probe, while the skin hydration was evaluated using a Corneometer® CM 825 probe, both of them being connected to a Multiprobe Adapter System (MPA5) from Courage-Khazaka (Koln, Germany).

2.15. Statistics

Data analyses were performed using IBM SPSS Software version 27.0.0.0 (Armonk, NY, USA). The continuous variables are presented as mean and standard error (SE). The dataset normality was assessed using the Kolmogorov-Smirnov (K-S) test followed by the ANOVA and Kruskal-Wallis tests. $p<0.05$ was considered statistically significant. The charts were modeled in Excel - Microsoft® Office Professional Plus 2019 from Microsoft Corp. (Washington, USA).

3. Results

3.1. Samples stability

Generally, the suspensions of polymer drug delivery systems based on different nano- and micro-particles are stable for months. The stability of samples is a key parameter that indicates the storage-controlled conditions such as humidity, temperature, sun exposure, etc. The changes of sample color and pH were within a very narrow range for all three samples at tested temperatures. **Table 1** displays the changes of the electrical conductivity.

Table 1. The changes of the electrical conductivity after 30 days.

Sample	Percentual changes at different temperature, %		
	8±0.5 °C	**25±0.5 °C**	**40±0.5 °C**
str 1	7.65	7.08	6.32
str 2	5.32	6.59	6.11
str 3	6.16	5.91	7.45

3.2. pH measurements

The evaluation of pH reveals the neutral and safe character of samples. The following results were obtained: 6.69±0.16 (sample str 1), 6.83±0.12 (str 2), and 6.78±0.08 (str 3).

3.3. Refractivity index

The values of refractivity index were: 1.59 for samples str 1 and str 3, and 1.61 for sample str 2.

3.4. Sample solubility

Table 2 presents the solubility of samples in different solvents.

Preprints (www.preprints.org) | NOT PEER-REVIEWED | Posted: 1 August 2023 doi:10.20944/preprints202308.0025.v1

Table 2. The solubility of samples.

Sample	Solubility (mg mL^{-1})		
	water	acetone	DMSO
str 1	0.86	1.04	1.05
str 2	0.84	1.11	1.02
str 3	0.90	1.09	1.06

3.5. Drug loading

The difference between the maximum absorbances of the carrier and the loaded active substance was used to determine the amount of free active substance; a graph absorbance vs calibration was drawn based on the absorbance of four standard solutions with different concentrations. Average encapsulation efficiencies equal to 67.2% (str 1), 68.9% (str 2) and 68.1% (str 3) were obtained by reporting the amount of free drug to the total quantity added to synthesis.

3.6. Drug release profile

The cumulated drug release is presented in Figure 2.

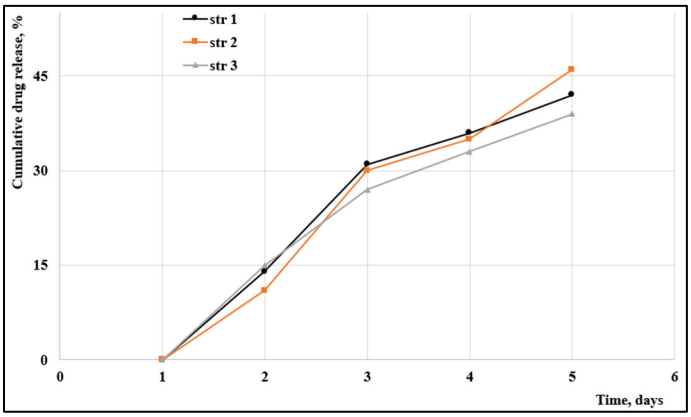

Figure 2. The evolution of the cumulated drug release.

3.7. Penetrability rate

The penetrability through various membranes is an important rate-limiting parameter that influences the release of the active agent to the target. A fast permeation through an artificial membrane was observed for all samples (Figure 3): almost 50% of particles penetrated in the first ten hours and around 70% passed through the membrane in the first 24h.

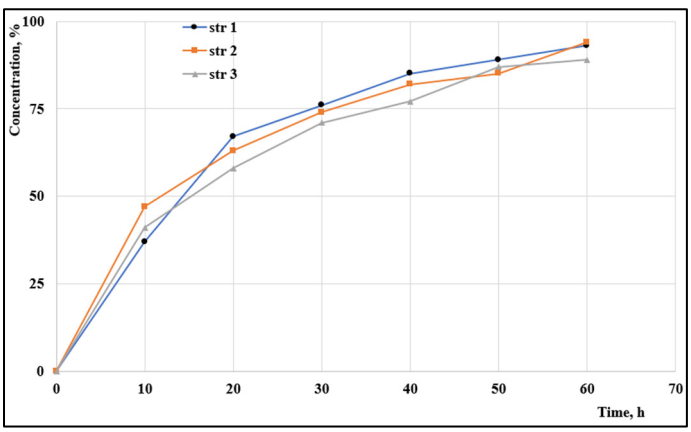

Figure 3. The penetrability rates.

Preprints (www.preprints.org) | NOT PEER-REVIEWED | Posted: 1 August 2023 doi:10.20944/preprints202308.0025.v1

3.8. FTIR-UATR

Figure 4 displays the FTIR spectra of the analyzed samples.

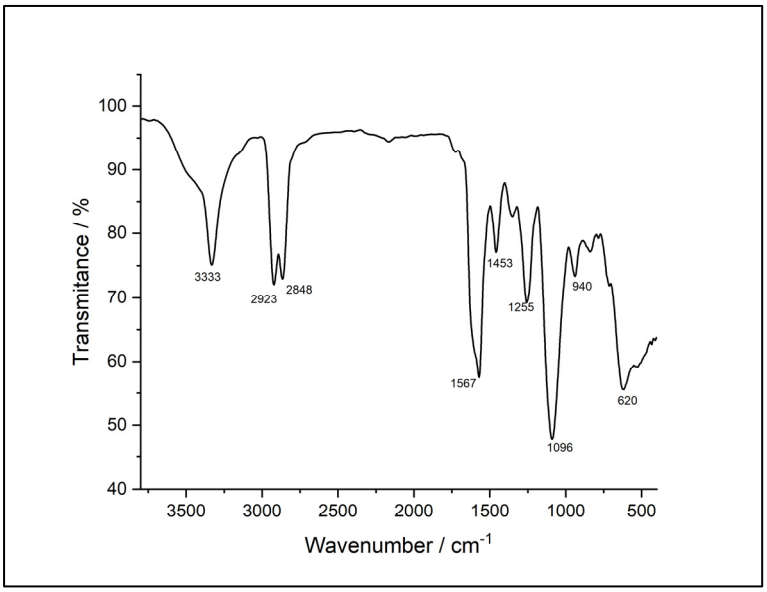

(**a**)

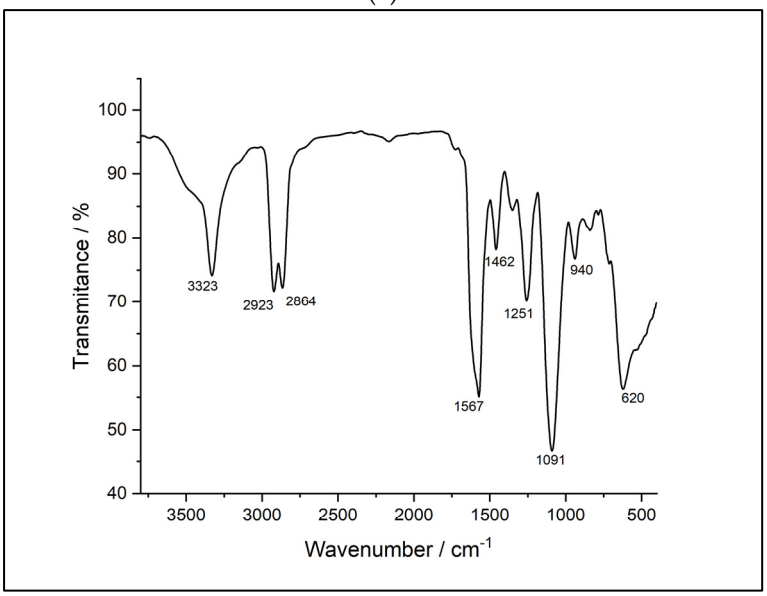

(**b**)

Preprints (www.preprints.org) | NOT PEER-REVIEWED | Posted: 1 August 2023 doi:10.20944/preprints202308.0025.v1

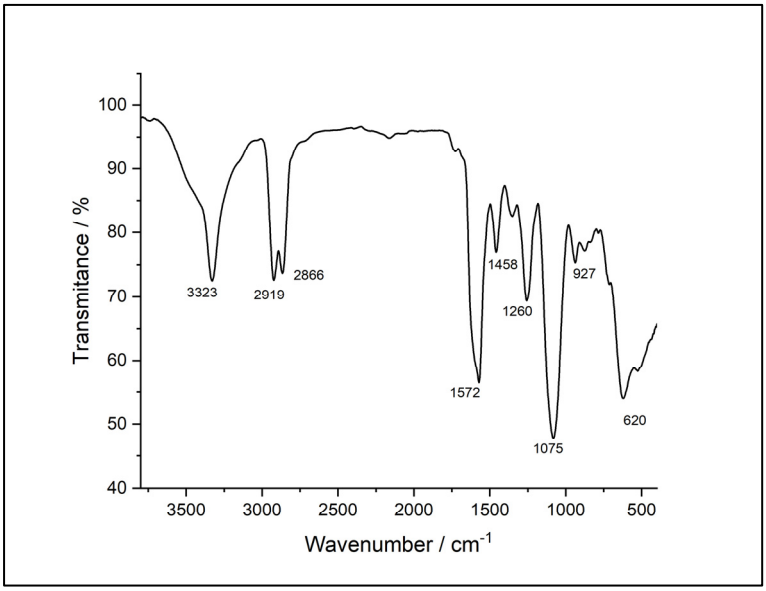

(**c**)

Figure 4. FTIR spectra of samples: (**a**) str 1, (**b**) str 2, and (**c**) str 3.

Comparatively, the FTIR-ATR spectra reveal many similarities between the synthesized samples. The spectra of the sample based on HDI (str 1) shows an absorption band at 3331 cm^{-1} corresponding to -NH- stretching. The two sharp bands at 2855 cm^{-1} and 2924 cm^{-1}, respectively, are associated with -CH_2- stretching, while displacements of the -CH_2- bond are indicated by the bands at 1460, 1440, 1353 and 1278 cm^{-1}. In addition, the absorption band specific to the urethane C=O bond occurs at 1734 cm^{-1}. The displacements of the -NH- bond appear at 1617 and 1577 cm^{-1}. The C-O-C bond can be identified by the presence of the bands at 1093 and 1075 cm^{-1}. There are also characteristic bands of primary or secondary aliphatic alcohols in the range of 1480-1405 cm^{-1} and 1075-1000 cm^{-1}. Mono-substituted alkyl ether-type structures are indicated by the presence of bands in the range of 1515-1455 cm^{-1}, 1260-1235 cm^{-1}, 1080-980 cm^{-1}, and 755-730 cm^{-1}.

The second sample (str 2) shows an absorption band, as in the case of the previous sample, at 3331 cm^{-1} corresponding to the -NH- stretch; two intense bands that can be attributed to the -CH_2- stretching occur at 2855 cm^{-1} and 2926 cm^{-1}, while the displacements of the -CH_2- bond are identified by 1460, 1438, 1352 and 1278 cm^{-1} bands. The absorption band specific to the urethane C=O bond is present at 1734 cm^{-1} and at 1670 cm^{-1}. The displacements of the -NH- bond appear at 1617 and 1577 cm^{-1}, respectively. The C-O-C bond is indicated by the presence of the bands at 1093 and 1075 cm^{-1}. There are also bands characteristic of primary or secondary aliphatic alcohols in the range of 1480-1405 cm^{-1}, and 1075-1000 cm^{-1}. Structures of the aliphatic cyclic ether-type can be identified by the bands within the 1400-1350 cm^{-1}, 1135-1050 cm^{-1}, 990-940 cm^{-1}, and 880-830 cm^{-1} ranges.

The FTIR spectra of sample str 3 contains an absorption band corresponding to the -NH- stretching at 3328 cm^{-1} and two intense bands that can be attributed to -CH_2- stretching at 2855 cm^{-1} and 2926 cm^{-1}, while the displacements of the -CH_2- bond are identified at 1460, 1438, 1352 and 1278 cm^{-1}. In addition, two absorption bands specific to the urethane C=O bond are present at 1734 cm^{-1} and at 1670 cm^{-1}, respectively, while the displacements of the -NH- bond appear at 1616 and 1576 cm^{-1}. The C-O-C bond is indicated by the presence of bands at 1090 and 1073 cm^{-1}. There are also bands characteristic of primary or secondary aliphatic alcohols in the range of 1480-1405 cm^{-1} and 1075-1000 cm^{-1}. Structures of the aliphatic cyclic ether-type can be identified by the occurrence of bands within the 1400-1350 cm^{-1}, 1135-1050 cm^{-1}, 990-940 cm^{-1}, and 880-830 cm^{-1} ranges.

Preprints (www.preprints.org) | NOT PEER-REVIEWED | Posted: 1 August 2023 doi:10.20944/preprints202308.0025.v1

3.9. Raman

Figure 5 reveals the Raman spectra of all three samples.

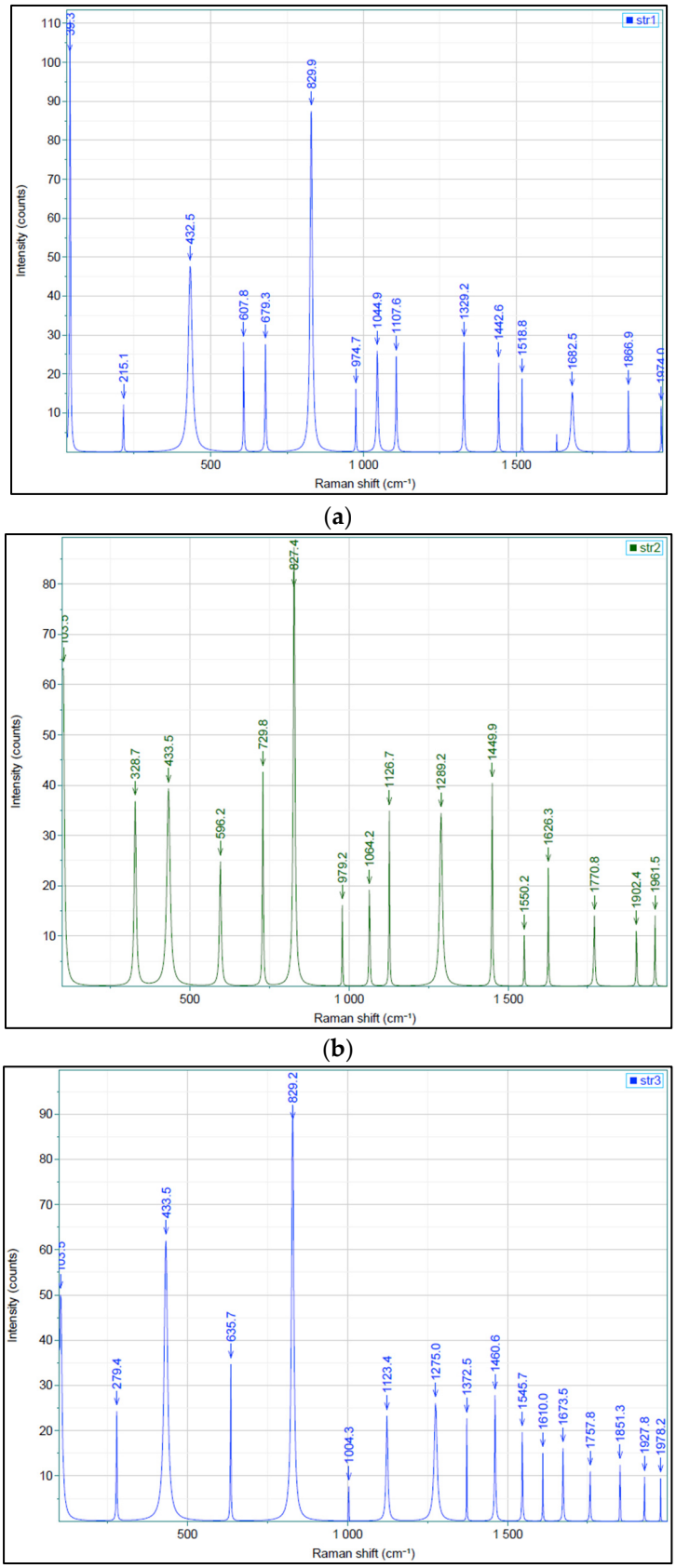

(**a**)

(**b**)

(**c**)

Figure 5. Raman spectra of samples: (**a**) str 1, (**b**) str 2, and (**c**) str 3.

Preprints (www.preprints.org) | NOT PEER-REVIEWED | Posted: 1 August 2023 doi:10.20944/preprints202308.0025.v1

The Raman spectra of samples show weak bands at 215.1 cm^{-1} (str 1) and 279.4 cm^{-1} (str 3) that correspond to the cleavage of C-C aliphatic bonds, a band between 432.5 cm^{-1} (str 1) and 433.5 cm^{-1} (str 2 and str 3) characteristic for several types of alcohols [25], bands between 596.2 cm^{-1} (str 2) and 635.7 cm^{-1} (str 3) attributed to the stretch of C-C alicyclic and aliphatic bonds. The C-O-C bond is indicated by the strong bands occurring between 827.4 and 829.9 cm^{-1}. The bands at 1329.2 and 1442.6 cm^{-1} (str 1), 1449.9 cm^{-1} (str 2), and 1372.5 and 1460.6 cm^{-1} (str 3) are associated with the stretch and asymmetric cleavage of $-CH_3$ and $-CH_2-$ bond. The stretch of C=O bonds is indicated by the presence of moderate bands within the range of 1626.3 cm^{-1} - 1682.5 cm^{-1}, while C-O-O- bonds were observed between 1757.8 cm^{-1} and 1770.8 cm^{-1}.

3.10. Thermal analysis

The following figures (Figures 6 and 7) present the results of different thermal analysis TG/DTG and DSC curves, respectively.

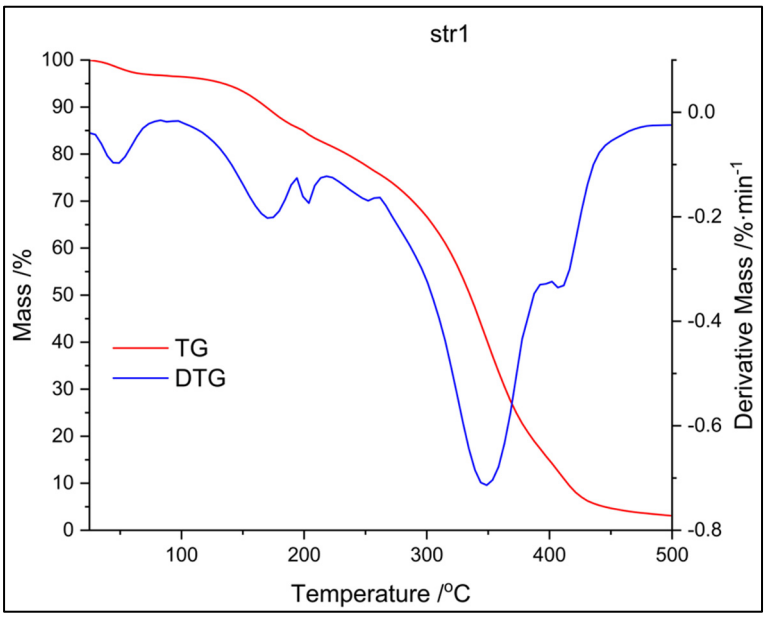

(**a**)

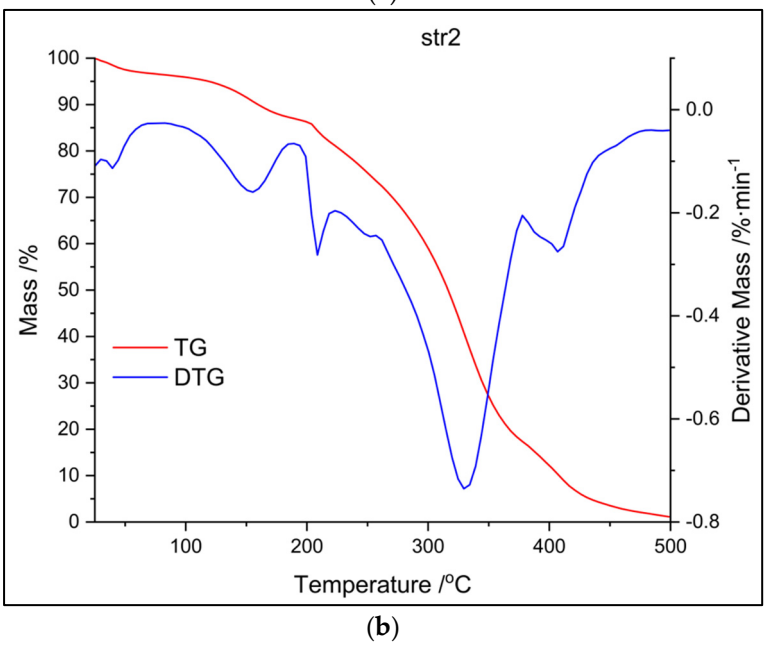

(**b**)

Preprints (www.preprints.org) | NOT PEER-REVIEWED | Posted: 1 August 2023 doi:10.20944/preprints202308.0025.v1

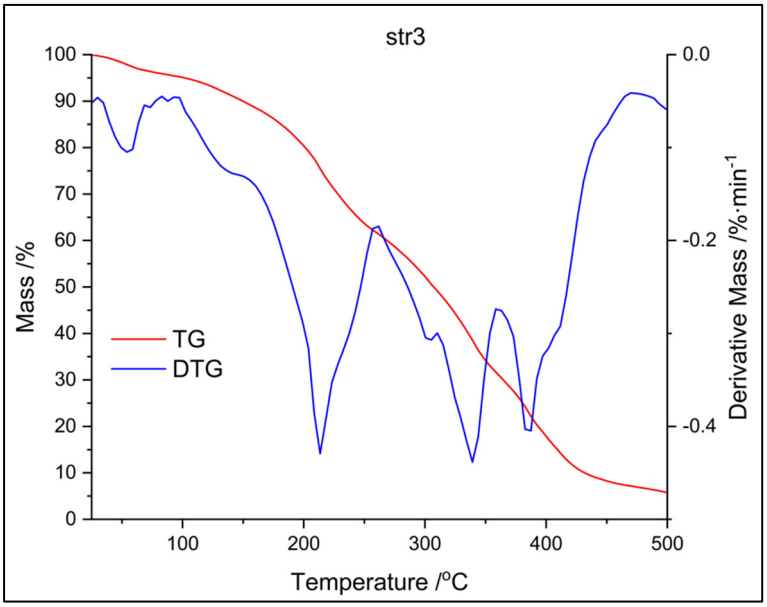

(**c**)

Figure 6. TG and DTG curves of samples: (**a**) str 1, (**b**) str 2, and (**c**) str 3.

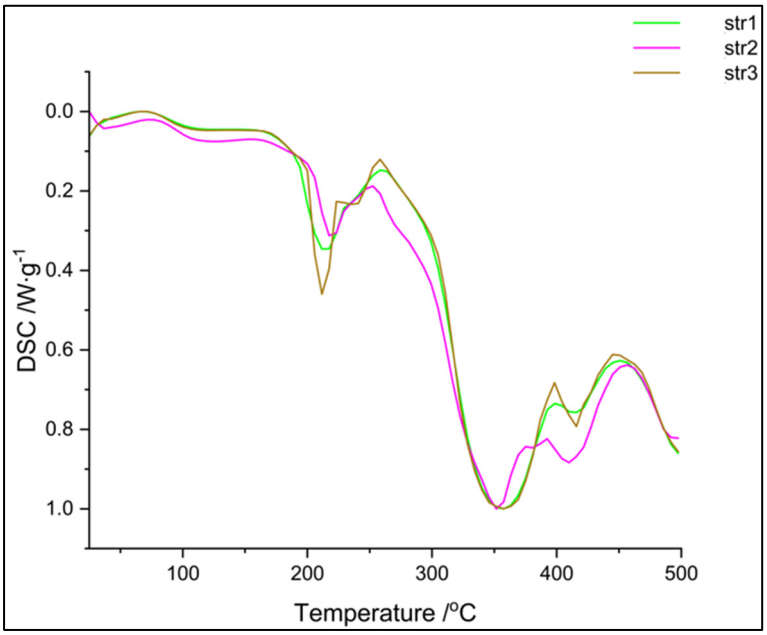

Figure 7. DSC curves of tested samples.

Thermal analysis (TG and DTG curves from Figure 6) shows that the decomposition of str 1 takes place within the same interval as for str 2 (an intense peak between 300 and 350 ˚C), while the third sample undergoes another two decomposition processes around 200 ˚C and 400 ˚C, respectively. A first stage of mass loss, below 100 ˚C for all samples, occurs due to water loss, while the decomposition between 200-400 ˚C can be attributed to the cleavage of PU linkage as previously described in the literature [26]. The decomposition of the carrier begins with a depolycondensation process and continues with the degradation of its hard segments (the part consisting of diisocyanate); the thermal degradation process is completed with the collapse of the soft segments from the macromolecular chains (the polyol part).

The DSC thermograms (Figure 7) confirm the data recorded in the previous thermal analysis. The samples are very similar, even if a different diisocyanate was used – two main endothermic peaks can be observed: a sharp one around 210 ˚C and a large one around 350 ˚C. The glass transition of

Preprints (www.preprints.org) | NOT PEER-REVIEWED | Posted: 1 August 2023 doi:10.20944/preprints202308.0025.v1

these materials was not observed within this temperature range; the literature reports the Tg of polyurethanes at negative values, between -60 and -20 °C, depending on the hard / soft segments ratio [27].

3.11. Zetasizer

Dynamic light scattering techniques were employed to assess the size and polydispersity of particles (PDI) as well as their surface charge. Table 3 presents the values obtained in the Zetasizer evaluations.

Table 3. The Zetasizer characterization of samples.

Sample	Analyzed parameters		
	size (nm)	PDI	Zeta potential (mV)
str 1	186±11 (81%) 145±7 (19%)	1.04	31.5±1.7
str 2	164±14 (100%)	1.11	28.3±1.2
str 3	190±12 (67%) 132±17 (33%)	1.09	30.0±1.6

The Zetasizer analyses (Table 3) has revealed the formation of disperse systems containing two particle populations for samples str 1 and 3 and one population for str 2; drug delivery systems based on disperse samples often assure a prolonged release due to their different degradation rate [28]. The average size of particles was very similar, ranging between 132 and 190 nm; the values of Zeta potential are specific to a colloidal system with moderate resistance against the tendency to form particles cluster; according to the literature, they are situated borderline between the values of nearly neutral and strongly cationic particles (28.3-31.5 mV) [29,30].

3.12. SEM Analysis

Figure 8 shows the SEM images of the surface morphology/micro-particles of tested samples.

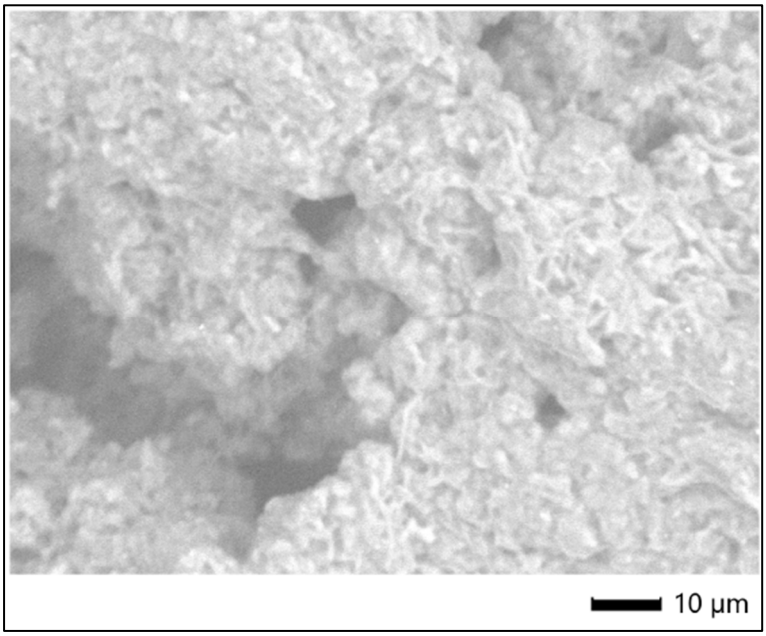

(**a**)

Preprints (www.preprints.org) | NOT PEER-REVIEWED | Posted: 1 August 2023 doi:10.20944/preprints202308.0025.v1

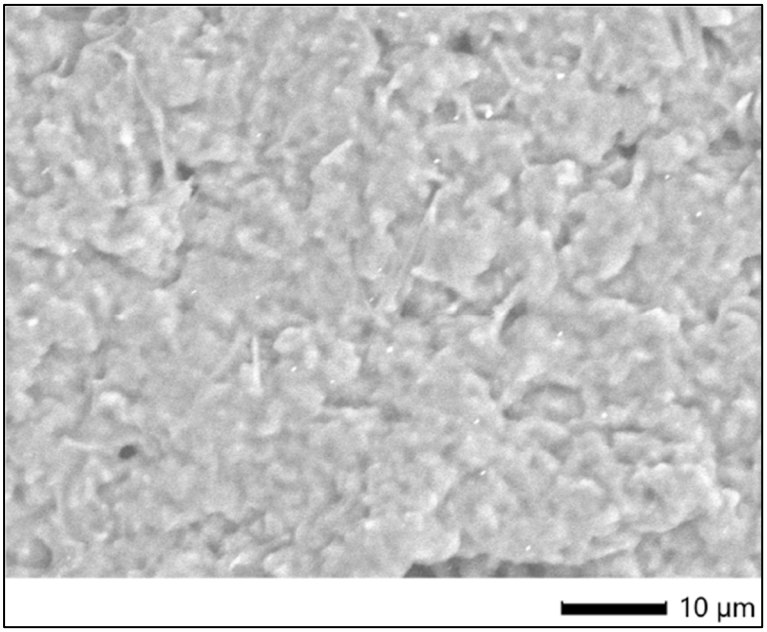

(**b**)

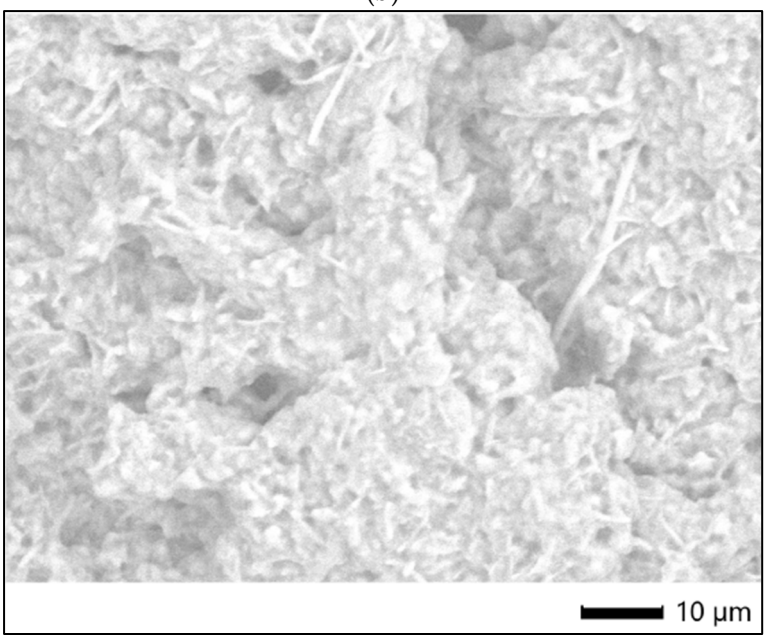

(**c**)

Figure 8. SEM images of tested samples: (**a**) str 1, (**b**) str 2, and (**c**) str 3.

3.13. Cells viability

Figure 9 presents the HDFa cells proliferation rate.

Preprints (www.preprints.org) | NOT PEER-REVIEWED | Posted: 1 August 2023 doi:10.20944/preprints202308.0025.v1

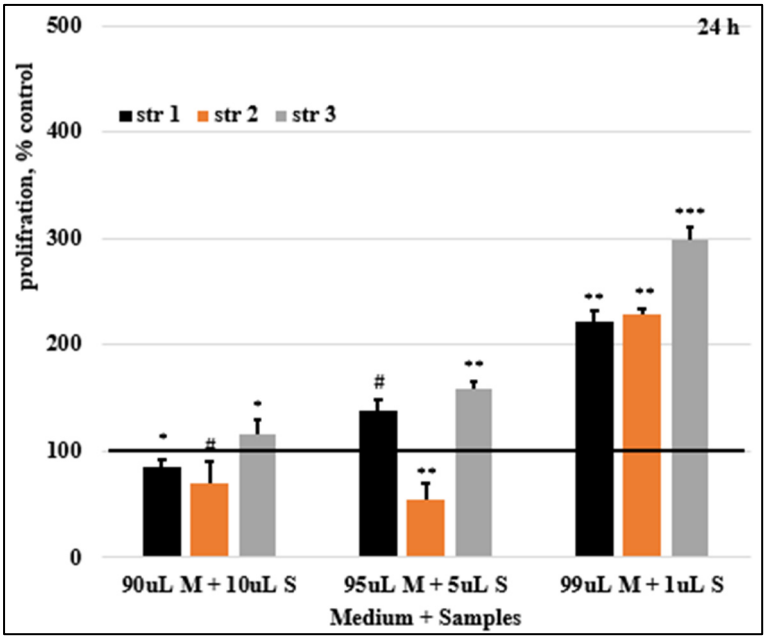

(a)

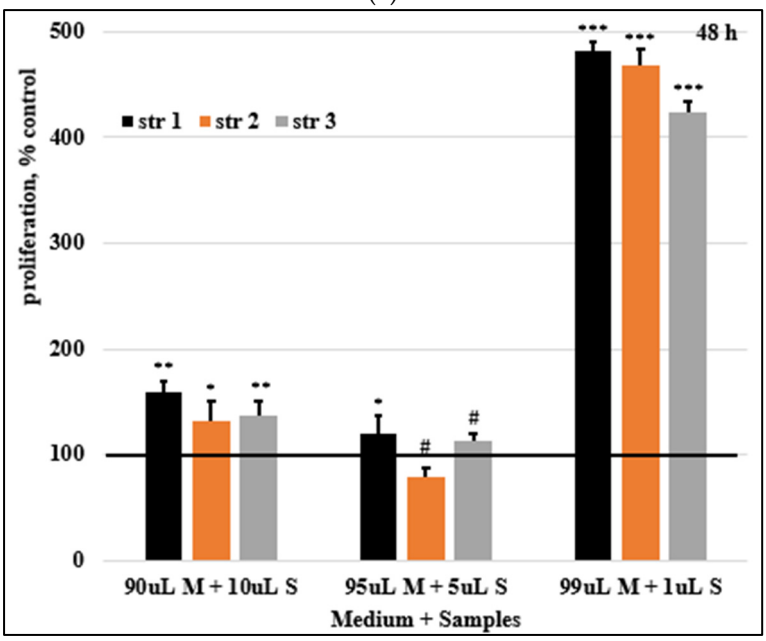

(b)

Preprints (www.preprints.org) | NOT PEER-REVIEWED | Posted: 1 August 2023 doi:10.20944/preprints202308.0025.v1

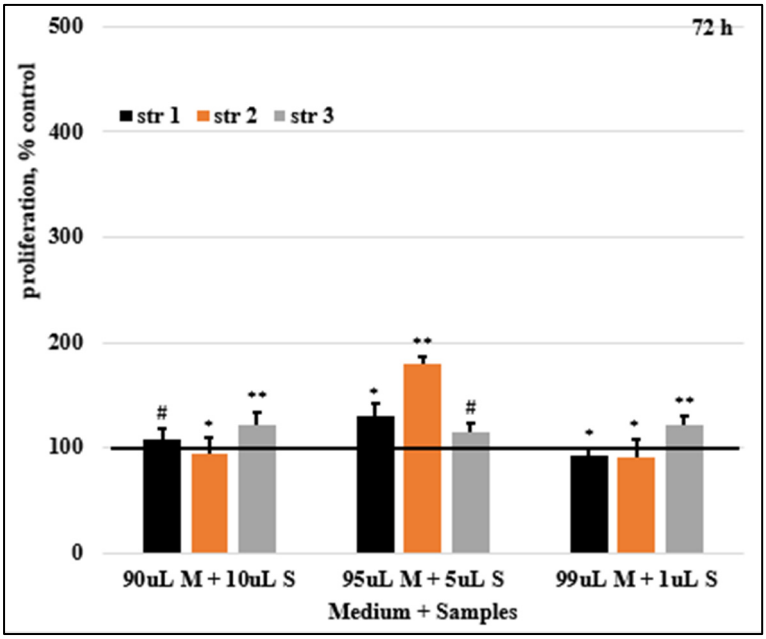

(**c**)

Figure 9. Cells proliferation rates after (**a**) 24, (**b**) 48, and (**c**) 72 hours. Control was set to 100%, # p> 0.05, * p< 0.05, ** p< 0.01, *** p< 0.001. Bars represent mean ± standard error of the mean.

The cells proliferation rates were studied at 24, 48 and 72 hours (Figure 9). After 24h, a reduced inhibition was observed at 10% sample str 1; sample str 2 exhibited an increased inhibition of cell proliferation, while for str 3 a stimulation of cells proliferation was recorded. Sample str 2 5% caused a marked decrease in cell proliferation, while in all other cases (at 5% and 1%), cell proliferation was stimulated.

At 48h post-exposure, with the exception of str 2 (at 5%), where a moderate inhibition can be seen, the stimulation of cell growth and development was noticed in all samples. At 72h incubation, str 2 (at 10%), as well as str 1 and str 2 (at 1%) produced an insignificant decrease in cell proliferation; in all the other samples, the same trend of stimulated cell proliferation can be observed.

3.14. Skin Irritation Evaluation

Two different mice strains were used in this research due to their different skin sensitivity; Figures 10 and 11 show the evolution of the main skin parameters (erythema and skin hydration) during the experiment.

Preprints (www.preprints.org) | NOT PEER-REVIEWED | Posted: 1 August 2023 doi:10.20944/preprints202308.0025.v1

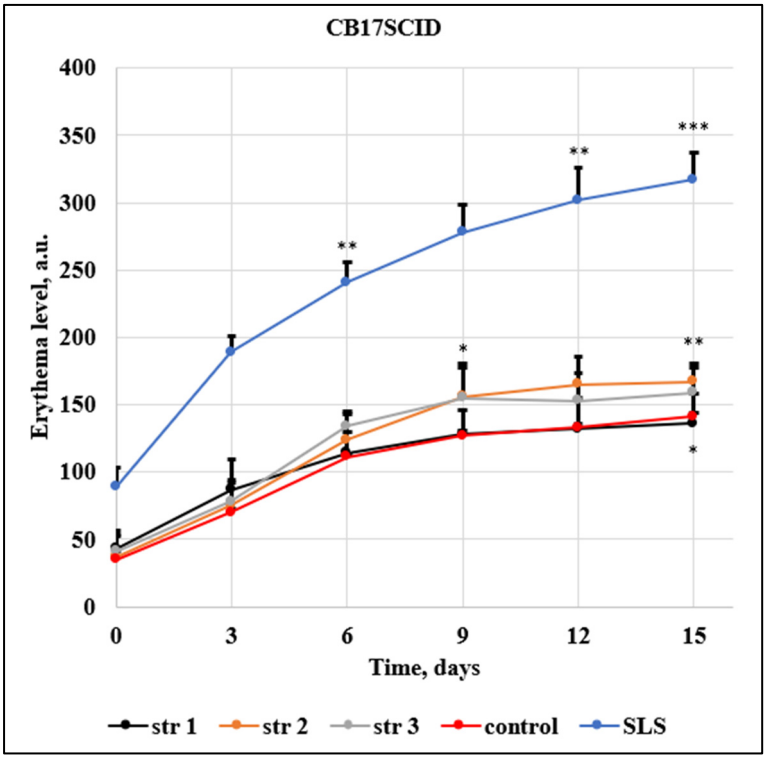

(**a**)

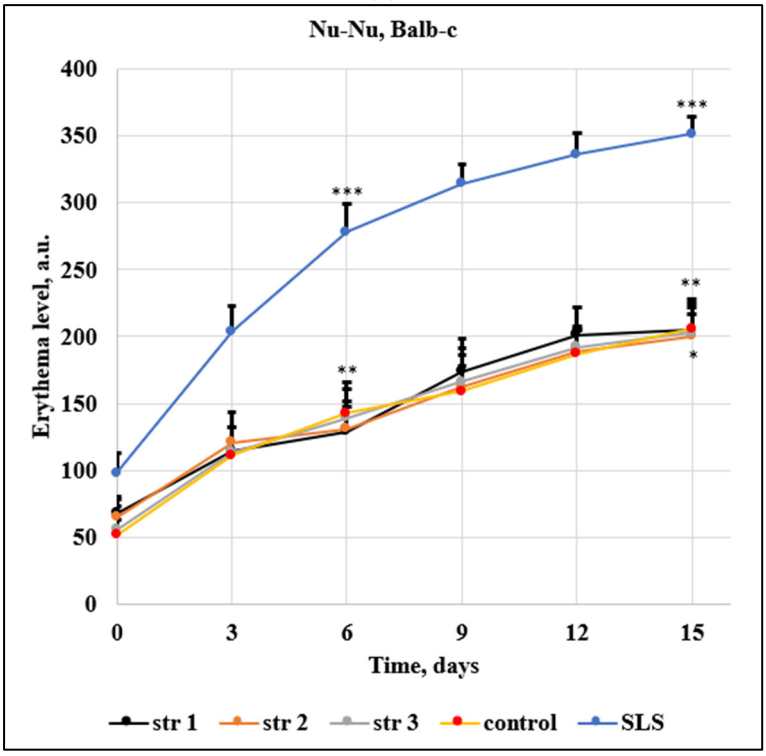

(**b**)

Figure 10. Evolution of erythema for (**a**) CB17SCID mice and (**b**) Balb-c, * $p< 0.05$, ** $p< 0.01$, *** $p< 0.001$. Bars represent mean ± standard error of the mean.

Preprints (www.preprints.org) | NOT PEER-REVIEWED | Posted: 1 August 2023 doi:10.20944/preprints202308.0025.v1

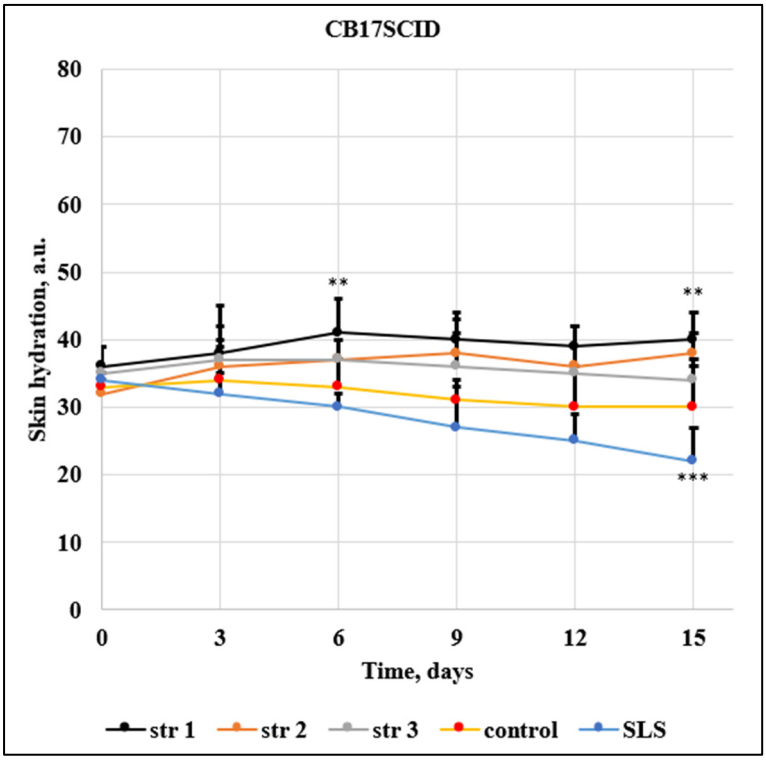

(**a**)

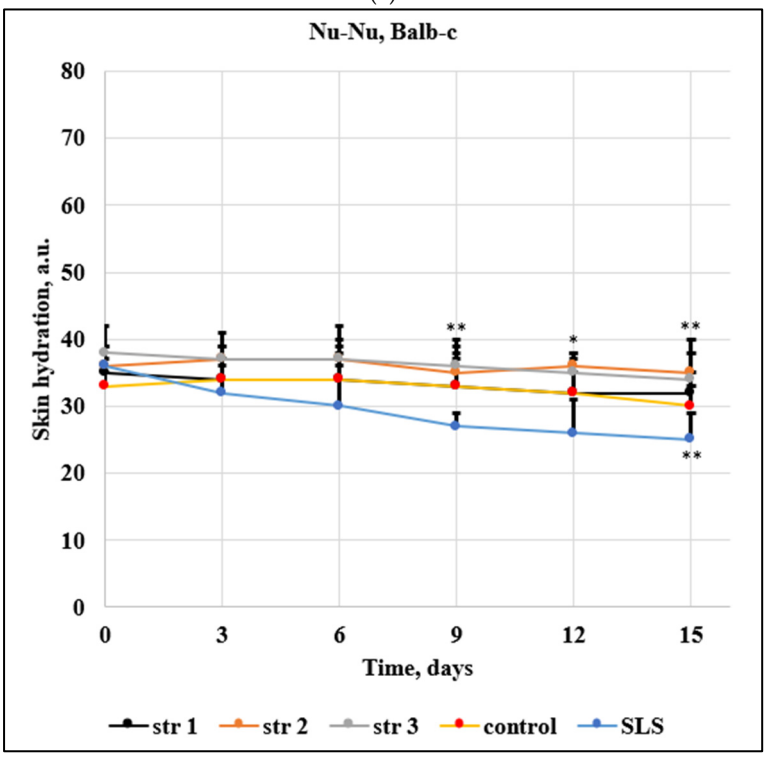

(**b**)

Figure 11. Evolution of the skin hydration for (**a**) CB17SCID mice and (**b**) Balb-c, * $p < 0.05$, ** $p < 0.01$, *** $p < 0.001$. Bars represent mean ± standard error of the mean.

Experimental mice represent successful research models in the development of new pharmaceuticals. The use of animals contributes to the advance of the scientific knowledge in developing and testing new drugs and therapies [31]. The mouse epidermis is often used as a model in skin pharmacology; skin irritations and cancer are studied on various strains of mice.

The following main parameters indicate a severe change of skin health: the increase of the transepidermal water loss and of the erythema level, combined with the decrease in skin hydration.

Preprints (www.preprints.org) | NOT PEER-REVIEWED | Posted: 1 August 2023 doi:10.20944/preprints202308.0025.v1

Of note, these parameters may vary significantly in the time unit; not every change can be associated with a health impairment or a sign of illness – this is the reason why the tested compounds are comparatively assessed against a known irritative compound. Erythema assessment (**Figure 10**) shows an increased level for all samples and for both mice strains (CB17SCID and Nu-Nu, Balb-c); for the first strain, the increase was max. 130 arb. units / 15 days for the PU samples – similar with control group (106 arb. units / 15 days), while sodium lauryl sulfate (that induce irritant contact dermatitis even at low concentrations, between 0.025% to 0.075%) has changed the erythema level by 228 arb. units / 15 days. The differences from the 1st to the 15th day are much larger for Nu-Nu, Balb-c mice due to their increased sensitivity.

The level of the skin hydration (Figure 11) has been modified only slightly in mice treated with the tested PU samples. The decrease of hydration was max. 1 arb. units / 15 days in the case of CB17SCID mice compared with 12 arb. units / 15 days (mice treated with SLS) and max. 3 arb. units / 15 days for Nu-Nu, Balb-c mice compared with 10 arb. units / 15 days (mice treated with SLS).

4. Discussion

Polymers are very frequently found as carrier materials in the administration of many drugs that pose various challenges such as low solubility and/or bioavailability, fast degradation, etc. [32,33]. The beginning of PU application in the pharmaceutical research field can be found in the last two decades of the last century, when a group from Japan has studied and reported the release behavior of crystal violet from a polyurethane gel [34], as well as the release of an antituberculous mixture (isoniazid, rifampicin, novocain) from a PU foam used as drug carrier matrixes [35].

The stability of pharmaceutical formulations is a very important parameter for the preservation of the active drug's bioavailability and to avoid chemical changes that may increase its toxic potential. Polyurethanes are very stable materials – a natural degradation of foams becomes visible only after 20-30 years [36]. However, there are known bacterial, thermal- and photo-oxidative processes that might contribute to their faster degradation. The current results indicate that the employed carrier is stable between 8 and 40 °C at 65% humidity for 30 days, a similar behavior with other PU samples described in the literature [17].

The pH of the synthesized samples, between 6.6 and 6.8, measured in aqueous solutions (0.8 mg mL^{-1}) is specific for nearly neutral products aimed for various administration routes. Generally, the pH of new formulations is maintained between 6 and 8 by using various buffer solutions in order to avoid altering the normal functioning of systems and tissues [37]. The narrow range of refractivity index (1.59-1.61) for the three samples indicates their similarity; the literature is rather poor in values of the refractivity index for polymer drug carriers, but M. Iwazumi and A. Schneider reported a larger range (1.53-1.63) for PU coatings [38], while J. Bauer *et al.* have reported higher values (1.55-1.75) for PU elastomer samples based on methylene-diphenyl diisocyanate and hexamethylene diisocyanate, respectively [39].

Aqueous solubility represents a significant drawback for PU carriers; we previously revealed this challenge [40] which was since improved only to a small extent. Thus, the water solubility of samples ranges between 0.84-0.90 mg mL^{-1}, in acetone (1.04-1.11 mg mL^{-1}) and in DMSO (1.02-1.06 mg mL^{-1}). Generally, drug carriers that show low aqueous solubilities are associated with delayed release [41], but this parameter is also influenced by the chemical structure of the delivery system according to the literature [42].

High values were found in the tested samples for the of dCMP encapsulation efficacy (between 67 and 69%); this parameter plays a major role in the design of drug delivery systems and it depends on the microencapsulation technique, the solubility of raw materials, the particle size, and the yield of the synthesis reaction. Another investigation on a PU carrier has revealed values of the encapsulation efficacy in a broad range between 55 and 85% [43], while Y. Batyrbekov and R. Iskakov [44] reported an even wider range for the values of entrapment efficiency of PU delivery systems (40-91%).

The cumulative drug release shows a similar trend that indicates the similarity between samples despite the particular isocyanate used. Almost 15% from the total amount was released after 48 hours

Preprints (www.preprints.org) | NOT PEER-REVIEWED | Posted: 1 August 2023 doi:10.20944/preprints202308.0025.v1

and around 45% after 5 days in which the samples were maintained in a degrading environment (a simulated body fluid previously described by T. Kokubo [20]. The kinetics can be described as a near linear release specific to a non-Fickian diffusion that were already met in other PU materials [45]. N. Abbasnezhad *et al.* have also reported a non-Fickian diffusion for PU-films loaded with diclofenac, but the mechanism depends on the film thickness [46].

The investigation of artificial membrane permeability is based on an artificial membrane, such as polyvinylidene difluoride which is widely used for immunoblotting techniques, and two compartments the so-called acceptor and donor chambers. The measurements provide different values of the permeability coefficients, known as percentage of flux or transported solute, which represents the part of the tested sample in the acceptor chamber. It was found that particles' penetrability through the artificial membrane was up to 50% in the first ten hours. It is currently known that the impermeability of the biological membranes is a major disadvantage in drug delivery due to its influence on the bioavailability of many drugs; the diffusion rate depends on particles' solubility, their size and surface charge. In the current research, almost the entire amount has passed through the artificial membrane within 60 hours.

The FT-IR evaluation was performed to find the possible interactions between the encapsulated substance and the polyurethane drug delivery system as well as to gain more data about the influence of the aliphatic diisocyanate structure on the properties of every sample; no significant difference was observed between the samples. Additionally, there are no traces of -NCO peak detected in the three samples obtained via polyaddition process and this indicates that the entire amount of diisocyanate has reacted completely to form polyurethane; the toxicity of isocyanate functional groups is widely known after the Bhopal gas tragedy from December 1984 when more than 500000 people were exposed to methyl isocyanate [47].

Raman spectroscopy was also used to assess the chemical structures of products and possible interactions. The complete reaction of isocyanate groups can be assumed by the presence the -C-N- single bond axial stretch (between 1518-1550 cm^{-1}) because the specific peak of -NCO groups does not appear in the observed range [48].

The investigation of the thermal behavior of polyurethane samples is very important due to the potentially hazardous chemicals which are released: a yellow smoke containing hydrogen cyanide and other toxic products was reported at temperatures above 600 °C [49]. The composition of the volatile compounds and residues arising PU thermal decomposition is influenced by the conditions of synthesis and the nature of the raw materials [50]. However, the safety of PU biomaterials is not a concern due to their high stability up to 300 °C according to the literature [51].

An assessment based on particles' velocity was involved to find the particles distribution size, respectively the electrophoretic mobility to analyze their tendency to form agglomerations. Repeated measurements on every sample have revealed that isocyanate structure does not affect much on the observed parameters. The dimensions of PU particles are between the limits recommended by the literature [52] and the values of the polydispersity index are highly corelated with the Zeta potentials.

In order to characterize the surface of PU particles, SEM analysis was employed; **Figure 8** shows semi-crystalline samples based on individual particles and agglomerates, that confirm the Zetasizer analysis.

Dermal fibroblasts are specialized cells, located deep in the skin, which generate connective tissue and help it to recover after an injury. The fibroblasts are often used in the evaluation of collagen production, identification of RNA mutations, and cytotoxicity as an indicator of bioincompatibility [53]. The analysis that was conducted in the present study consists of the cell viability assessment of samples in human dermal fibroblasts. The data obtained indicated similar trends among the samples despite their differences. Based on the results obtained, it can be stated that this PU delivery system could be considered a good possible choice for further *in vivo* evaluation.

An *in vivo* non-invasive and quantitative study of erythema and skin hydration level was included in this research to investigate if the synthesized products present irritative effects. M. Denzinger et al. consider that modifications in the level of skin hydration are detectable before the appearance of erythema change. [54]. Despite the slight increase of erythema and decrease of skin

Preprints (www.preprints.org) | NOT PEER-REVIEWED | Posted: 1 August 2023 doi:10.20944/preprints202308.0025.v1

hydration during assessment, the results obtained in this study indicate that the synthesized products not alter the epidermal function, respectively the strong correlation between two skin parameters. A. Chireanu et al. describe a similar drug delivery system based on polyester-urethane microparticles used for curcumin and they report similar differences of skin parameters between the samples and reference (sodium lauryl sulfate) [55].

Collectively, the *in vitro* and *in vivo* assessments of the currently synthesized drug delivery systems have revealed that these products are safe to be used in further clinical trials.

5. Conclusions

Polyurethanes have been discovered by Prof. Otto Bayer almost 90 years ago and they are still in development by many industries under various forms, from elastomers and rigid foams, coatings and insulation materials to heart valves, artificial skin, arteries and veins, wound dressing materials and long-term implants. This paper introduces the synthesis and preliminary characterization of a PU drug delivery system that combines different degradation pathways (hydrolytic and enzymatic types based on the ester functional groups, oxidative, physical and enzymatic types based on the ether groups and enzymatic and hydrolytic types based on urethane functional groups) in order to obtain a drug carrier with a controlled release. The characterization of the samples indicates the preparation of a carrier able to encapsulate large amounts of nucleosides, with a prolonged release and good penetrability rate.

The inexpensive materials and the mild reaction conditions that are specific to the sustainable or green chemistry on one hand, combined with the easiness to modulate the particle size by changing the ratio between the main polyol / polyols and the chain extenders on the other hand, make these polymers attractive materials for drug delivery. Their biodegradability and long-term biocompatibility, already validated by previous studies, add to their potential use as drug carries.

Author Contributions: Conceptualization, F.B. and C.M.S.; methodology, T.V.; software, F.B.; validation, G.V. and R.P.; formal analysis, G.V.; investigation, T.V.; resources, F.B.; data curation, R.P.; writing—original draft preparation, F.B.; writing—review and editing, T.V.; visualization, R.P.; supervision, C.M.S.; project administration, F.B.; funding acquisition, F.B. All authors have read and agreed to the published version of the manuscript.

Funding: This research was funded by "Victor Babes" University of Medicine and Pharmacy Timisoara, grant number 5EXP/1244/ 30.01.2020.

Institutional Review Board Statement: The study was conducted in accordance with the Declaration of Helsinki, and approved by the Institutional Review Board (or Ethics Committee) of "Victor Babes" University of Medicine and Pharmacy Timisoara (approval no. 42 from October 29th, 2021).

Conflicts of Interest: The authors declare no conflict of interest.

References

1. Huang, R.M.; Chen, Y.N.; Zeng, Z.; Gao, C.H.; Su, X.; Peng, Y. Marine nucleosides: Structure, bioactivity, synthesis and biosynthesis. *Marine Drugs* **2014**, *12*(12), 5817-5838.
2. Fu, J.; Wu, Z.; Zhang, L. Clinical applications of the naturally occurring or synthetic glycosylated low molecular weight drugs. In: *Progress in Molecular Biology and Translational Science*; Teplow, D.B., Eds.; Academic Press Inc.: Amsterdam, Netherlands, 2019, 163, pp. 487-522.
3. Yegutkin, G.G. Adenosine metabolism in the vascular system. *Biochem. Pharmacol.* **2021**, *187*, 114373.
4. Villa, E.; Ali, E.S.; Sahu, U.; Ben-Sahra, I. Cancer cells tune the signaling pathways to empower de novo synthesis of nucleotides. *Cancers* **2019**, 11(5), 688.
5. Rawat, R.S.; Kumar, S. (2023) Understanding the mode of inhibition and molecular interaction of taxifolin with human adenosine deaminase. *J. Biomol. Struct. Dyn.* **2023**, *41*(2), 377-385.
6. Teng, H.; Wang, Y.; Sui, X.; Fan, J.; Li, S.; Lei, X.; Shi, C.; Sun, W.; Song, M.; Wang, H.; Dong, D.; Geng, J.; Zhang, Y.; Zhu, X.; Cai, Y.; Li, Y.; Li, B.; Min, Q.; Wang, W.; Zhan, Q. Gut microbiota-mediated nucleotide synthesis attenuates the response to neoadjuvant chemoradiotherapy in rectal cancer. *Cancer Cell.* **2023**, *41*(1), 124-138.e6.

Preprints (www.preprints.org) | NOT PEER-REVIEWED | Posted: 1 August 2023 doi:10.20944/preprints202308.0025.v1

7. Tan, C.L. Facts Cannot be Ignored When Considering the Origin of Life# 2: Challenges in Generating the First Gene-encoding Template DNA or RNA. *Answers Res. J.* **2022**, *15*, 31-48.
8. Martikainen, L.; Walther, A.; Ikkala, O. Cytidine Functionalization Promotes Synergistic Mechanical Properties in Nacre-Mimetic Nanocomposites. In Proceedings of International Conference on Composite Materials, Montreal, Canada, July 28 - August 2, 2013 (pp. 1358-1365).
9. Studzińska, S.; Buszewski, B. Effect of mobile phase pH on the retention of nucleotides on different stationary phases for high-performance liquid chromatography. *Anal. Bioanal. Chem.* **2013**, *405*, 1663-1672.
10. Wendels, S.; Avérous, L. Biobased polyurethanes for biomedical applications. *Bioact. Mater.* **2021**, *6*(4), 1083-1106.
11. Gawlikowski, M.; El Fray, M.; Janiczak, K.; Zawidlak-Węgrzyńska, B.; Kustosz, R. In-vitro biocompatibility and hemocompatibility study of new PET copolyesters intended for heart assist devices. *Polymers* **2020**, *12*(12), 2857.
12. Singh, S.; Kumar Paswan, K.; Kumar, A.; Gupta, V.; Sonker, M.; Ashhar Khan, M.; Kumar, A.; Shreyash, N. Recent Advancements in Polyurethane-based Tissue Engineering. *ACS Appl. Bio Mater.* **2023**, *6*(2), 327-348.
13. Bouchemal, K.; Briançon, S.; Perrier, E.; Fessi, H.; Bonnet, I.; Zydowicz, N. Synthesis and characterization of polyurethane and poly(ether urethane) nanocapsules using a new technique of interfacial polycondensation combined to spontaneous emulsification. *Int. J. Pharm.* **2004**, *269*(1), 89-100.
14. Bouchemal, K.; Briançon, S.; Perrier, E.; Fessi, H. Nano-emulsion formulation using spontaneous emulsification: solvent, oil and surfactant optimisation. *Int. J. Pharm.* **2004**, *280*(1-2), 241-251.
15. Bouchemal, K.; Briançon, S.; Couenne, F.; Fessi, H.; Tayakout, M. Stability studies on colloidal suspensions of polyurethane nanocapsules. *J. Nanosci. Nanotechnol.* **2006**, *6*(9-10), 3187-3192.
16. Borcan, L.-C.; Dudas, Z.; Len, A.; Fuzi, J.; Borcan, F.; Tomescu, M.C. Synthesis and characterization of a polyurethane carrier used for a prolonged transmembrane transfer of a chili pepper extract. *Int. J. Nanomed.* **2018**, *13*, 7155-7166.
17. Borcan, F.; Chirita-Emandi, A.; Andreescu, N.I.; Borcan, L.-C.; Albulescu, R.C.; Puiu, M.; Tomescu, M.C. Synthesis and preliminary characterization of polyurethane nanoparticles with ginger extract as a possible cardiovascular protector, *Int. J. Nanomed.* **2019**, *14*, 3691-3703.
18. Munteanu, M.F.; Ardelean, A.; Borcan, F.; Trifunschi, S.I.; Gligor, R.; Ardelean, S.A.; Coricovac, D.; Pinzaru, I.; Andrica, F.; Borcan, L.-C. Mistletoe and Garlic Extracts as Polyurethane Carriers – A Possible Remedy for Choroidal Melanoma. *Curr. Drug Deliv.* **2017**, *14*(8), 1178-1188.
19. Borcan, F.; Len, A.; Bordejevic, D.A.; Dudas, Z.; Tomescu, M.C.; Valeanu, A.N. Obtaining and characterization of a polydisperse system used as a transmembrane carrier for isosorbide derivatives. *Front. Chem.* **2020**, *8*, 492.
20. Borcan, F.; Len, A.; Dehelean, C.A.; Dudás, Z.; Ghiulai, R.; Iftode, A.; Racoviceanu, R.; Soica, C.M. Design and Assessment of a Polyurethane Carrier Used for the Transmembrane Transfer of Acyclovir. *Nanomaterials (Basel)* **2021**, *11*(1), 51.
21. Tuta-Sas, I.; Borcan, F.; Sas, I. Synthesis and preliminary characterization of polyurethane matrices used as a drug carrier for bromelain. *Mater. Plast.* **2023**, *60*(1), 1-12.
22. Citu, C.; Ceuta, L.; Popovici, R.; Ionescu, D.; Pinzaru, I.; Borcan, F. Alternative Possibilities to Asses a Phytohormone Release Rate from a Polyurethane Carrier. *Mater. Plast.* **2015**, *52*(4), 553-559.
23. Moleriu, L.; Duse, A.O.; Borcan, F.; Soica, C.; Kurunczi, L.; Nicolov, M.; Mioc, M. Formulation and characterization of antibacterial hydrogels based on polyurethane microstructures and 1,2,4-triazole derivatives. *Mater. Plast.* **2017**, *54*(2), 348-352.
24. Baino, F.; Yamaguchi, S. The Use of Simulated Body Fluid (SBF) for Assessing Materials Bioactivity in the Context of Tissue Engineering: Review and Challenges. *Biomimetics (Basel)* **2020**, *5*(4), 57.
25. Lin-Vien, D.; Colthup, N.B.; Fateley, W.G.; Grasselli, J.G. Alcohols and Phenols. In: *The Handbook of Infrared and Raman Characteristic Frequencies of Organic Molecules*; Lin-Vien, D.; Colthup, N.B.; Fateley, W.G.; Grasselli, J.G., Eds.; Academic Press Inc., Amsterdam, Netherland, 1991, pp. 45-60.
26. Lopes, R.V.V.; Osorio, L.F.B.; Santos, M.L.; Sales, M.J.A. Characterization of Polyurethanes from Vegetable Oils by TG/DTG, DMA and FT-IR. *Macromolec. Symposia* **2012**, *319*(1).
27. Son, T.W.; Lee, D.W.; Lim, S.K. Thermal and Phase Behavior of Polyurethane Based on Chain Extender, 2,2-Bis-[4-(2-hydroxyethoxy)phenyl]propane. *Polym. J.* **1999**, *31*(7), 563-568.
28. Peterson, G.I.; Ko, W.; Hwang, Y.J.; Choi, TL. Mechanochemical Degradation of Amorphous Polymers with Ball-Mill Grinding: Influence of the Glass Transition Temperature. *Macromolecules* **2020**, *53*(18), 7795-7802.

Preprints (www.preprints.org) | NOT PEER-REVIEWED | Posted: 1 August 2023 doi:10.20944/preprints202308.0025.v1

29. Salopek, B.; Krasic, D.; Filipovic, S. Measurement and application of zeta-potential. *Rudarsko-geolosko-naftni zbornik* **1992**, *4*(1), 147.
30. Clogston, J.D.; Patri, A.K. Zeta potential measurement. *Methods Mol. Biol.* **2011**, *697*, 63-70.
31. Lemon, R.; Dunnett, S.B. Surveying the literature from animal experiments. *BMJ* **2005**, *330*(7498), 977-978.
32. Begines, B.; Ortiz, T.; Pérez-Aranda, M.; Martínez, G.; Merinero, M.; Argüelles-Arias, F.; Alcudia, A. Polymeric Nanoparticles for Drug Delivery: Recent Developments and Future Prospects. *Nanomaterials (Basel)* **2020**, *10*(7), 1403.
33. Elmowafy, M.; Shalaby, K.; Elkomy, M.H.; Alsaidan, O.A.; Gomaa, H.A.M.; Abdelgawad, M.A.; Mostafa, E.M. Polymeric Nanoparticles for Delivery of Natural Bioactive Agents: Recent Advances and Challenges. *Polymers* **2023**, *15*, 1123.
34. Kohjiya, S.; Ikeda, Y.; Takesako, S.; Yamashita, S. Drug release behavior from polyurethane gel. *React. Polym.* **1991**, *15*, 165-175.
35. Batyrbekov, E.O; Moshkevich, S.A.; Rukhina, L.B.; Bogin, R.A.; Zhubanov, B.A. Some fields of biomedical application of polyurethanes. *Polym. Int.* **1990**, *23*(3), 273-276.
36. Bhuvaneswari, H. Degradability of Polymers. In: *Recycling of Polyurethane Foams*; Sabu, T.; Ajay V.R.; Krishnan K.; Abitha, V.K.; Martin, G.T., Eds.; William Andrew Publishing, Norwich, NY, 2018; pp. 29-44.
37. Abdella, S.; Abid, F.; Youssef, S.H.; Kim, S.; Afinjuomo, F.; Malinga, C.; Song, Y.; Garg, S. pH and its applications in targeted drug delivery. *Drug Discov. Today* **2023**, *28*(1), 103414.
38. Iwazumi, M.; Schneider, A. High refractive index aqueous polyurethane dispersion coating compositions. WO2011163461A1, **2011**.
39. Bauer, J.; Gutke, M.; Heinrich, F.; Edling, M.; Stoycheva, V.; Kaltenbach, A.; Burkhardt, M.; Gruenefeld, M.; Gamp, M.; Gerhard, C.; Steglich, P.; Steffen, S.; Herzog, M.; Dreyer, C.; Schrader, S. Novel UV-transparent 2-component polyurethane resin for chip-on-board LED micro lenses. *Opt. Mater. Express* **2020**, *10*, 2085-2099.
40. Citu, I.M.; Borcan, F.; Zambori, C.; Tita, B.; Paunescu, V.; Ardelean, S. Influence of crosslinking agent - chain extender ratio on the properties of hyperbranched polyurethane structures used as dendritic drug carrier. *Rev. Chim. Bucharest* **2015**, *66*(1), 119-123.
41. Tekade, A.R.; Yadav, J.N. A Review on Solid Dispersion and Carriers Used Therein for Solubility Enhancement of Poorly Water Soluble Drugs. *Adv. Pharm. Bull.* **2020**, *10*(3), 359-369.
42. Józó, M.; Simon, N.; Yi, L.; Móczó, J.; Pukánszky, B. Improved Release of a Drug with Poor Water Solubility by Using Electrospun Water-Soluble Polymers as Carriers. *Pharmaceutics* **2022**, *14*(1), 34.
43. Javidi, M.; Fathi Fathabadi, H.; Jenabali Jahromi, S.A.; Khorram, M. Investigating the interfacial synthesis of polyurethane microcapsules and optimization of the process using response surface method. *Mater. Res. Express* **2019**, *6*(10), 105302.
44. Batyrbekov, Y.; Iskakov, R. Polyurethane as Carriers of Antituberculosis Drugs. In: *Polyurethane*; Zafar, F.; Sharmin E., Eds.; IntechOpen, Rijeka, Croatia, 2012.
45. Fu, Y.; Kao, W.J. Drug release kinetics and transport mechanisms of non-degradable and degradable polymeric delivery systems. *Expert Opin Drug Deliv.* **2010**, *7*(4), 429-444.
46. Abbasnezhad, N.; Zirak, N.; Shirinbayan, M.; Kouidri, S.; Salahinejad, E.; Tcharkhtchi, A.; Bakir, F. Controlled release from polyurethane films: Drug release mechanisms. *J. Appl. Polym. Sci.* **2020**, *12*, 50083.
47. Varma, R.; Varma, D.R. The Bhopal Disaster of 1984. *Bull. Sci. Technol. Soc.* **2005**, *25*(1), 37-45.
48. da Cunha, F.O.V.; Melo, D.H.R.; Veronese, V.B.; Forte, M.M.C. Study of castor oil polyurethane-poly(methyl methacrylate) semi-interpenetrating polymer network (SIPN) reaction parameters using a 2^3 factorial experimental design. *Mater. Res. Ibero-Am.* **2004**, *7*(4), 539-543.
49. Chambers, J.; Jirickny, J.; Reese, C. The thermal decomposition of polyurethanes and polyisocyanurates. *Fire Mater.* **1981**, *5*(4), 133-141.
50. Amado, J.C.Q. Thermal Resistance Properties of Polyurethanes and Its Composites. In: *Thermosoftening Plastics*; Evingür, G.A.; Pekcan, O.; Achilias, D.S., Eds.; IntechOpen, Rijeka, 2023.
51. Bolcu, C.; Borcan, F.; Nutiu, R. Aspects regarding the synthesis and characterization of some types of thermoplastic polyurethanes. *Mater. Plast.* **2006**, *43*, 258-261.
52. Peng, T.; Lin, S.; Niu, B.; Wang, X.; Huang, Y.; Zhang, X.; Li, G.; Pan, X.; Wu, C. Influence of physical properties of carrier on the performance of dry powder inhalers. *Acta Pharm Sin B.* **2016**, *6*(4), 308-318.

Preprints (www.preprints.org) | NOT PEER-REVIEWED | Posted: 1 August 2023 doi:10.20944/preprints202308.0025.v1

53. Schmidt, R.J.; Chung, L.Y.; Andrews, A.M.; Turner, T.D. Toxicity of L-ascorbic acid to L929 fi-broblast cultures: relevance to biocompatibility testing of materials for use in wound management. *J Biomed Mater Res.* **1993**, *27*(4), 521-530.
54. Denzinger, M.; Krauss, S.; Held, M.; Joss, L.; Kolbenschlag, J.; Daigeler, A.; Rothenberger, J. A quantitative study of hydration level of the skin surface and erythema on conventional and microclimate management capable mattresses and hospital beds. *J Tissue Viability* **2020**, *29*(1), 2-6.
55. Chioreanu, A.; Mot, I.C.; Horhat, D.I.; Balica, N.C.; Sarau, C.A.; Morar, R.; Domuta, E.M.; Dumitru, C.; Negrean, R.A.; Bumbu, B.A.; Ravulapalli, M.; Alambaram, S.; Akshay, R.; Pricop, M. Development and Preliminary Characterization of Polyester-Urethane Microparticles Used in Curcumin Drug Delivery System for Oropharyngeal Cancer. *Medicina* **2022**, *58*, 1689.

Disclaimer/Publisher's Note: The statements, opinions and data contained in all publications are solely those of the individual author(s) and contributor(s) and not of MDPI and/or the editor(s). MDPI and/or the editor(s) disclaim responsibility for any injury to people or property resulting from any ideas, methods, instructions or products referred to in the content.